https://doi.org/10.15407/ufm.25.03.459

B.V. BORTS*, O.O. PARKHOMENKO, V.V. GANN***, A.Yu. ZELINSKY****, V.I. SYTIN, I.O. VOROBYOV, L.I. GLUSCHENKO, I.I. KARNAUKHOV, Yu.O. MARCHENKO, AND M.P. DOMNICH**

National Scientific Centre 'Kharkiv Institute of Physics and Technology' of the N.A.S. of Ukraine,
1 Akademichna Str., UA-61108 Kharkiv, Ukraine

* borts@kipt.kharkov.ua, ** parkhomenko@kipt.kharkov.ua,
*** gann@kipt.kharkov.ua, **** zelinsky@kipt.kharkov.ua

PROPERTIES OF W–Ta MATERIALS OF THE NEUTRON-PRODUCING TARGET OF THE SUBCRITICAL ASSEMBLY AT THE NATIONAL SCIENTIFIC CENTRE 'KHARKIV INSTITUTE OF PHYSICS AND TECHNOLOGY' OF THE NATIONAL ACADEMY OF SCIENCES OF UKRAINE

The works in the field of radiation materials science of target materials of neutron sources based on the subcritical assemblies controlled by linear accelerators of electrons or protons, so-called accelerator driven systems (ADS), are reviewed. Now, electronuclear ADS systems are the prototype of safe nuclear reactors of the 5th generation. In connection with the physical start-up of the neutron source facility of the National Scientific Centre 'Kharkiv Institute of Physics and Technology' of the N.A.S. of Ukraine (NSC 'KhIPT' NASU), the target of which is fabricated from powdered tungsten covered with tantalum, the issues of preparation technology, construction, and physical and mechanical properties of W–Ta materials of targets in non-irradiated and irradiated states are considered. The nuclear-physical processes of radiation damage to the target during co-irradiation of it with both neutrons of a subcritical assem-

Citation: B.V. Borts, O.O. Parkhomenko, V.V. Gann, A.Yu. Zelinsky, V.I. Sytin, I.O. Vorobyov, L.I. Gluschenko, I.I. Karnaukhov, Yu.O. Marchenko, and M.P. Domnich, Properties of W–Ta Materials of the Neutron-Producing Target of the Subcritical Assembly at the National Scientific Centre 'Kharkiv Institute of Physics and Technology' of the National Academy of Sciences of Ukraine, *Progress in Physics of Metals*, **25**, No. 3: 459–481 (2024)

bly and high-energy *e*- and γ-beams are analyzed. The target resources of ADS systems are estimated. As noted, the difficulty of predicting the 'survivability' of the W–Ta target also relates to the fact that, except for the works carried out at the NSC 'KhIPT' NASU in 70–90th of the last century, there are no experimental works in the world on the radiation damage of reactor materials by high-energy electrons with an energy of 100 MeV and above.

Keywords: subcritical nuclear systems, tungsten–tantalum targets, high-temperature vacuum rolling, mechanical properties, metallography, nano- and microhardness, level of damage, radiation embrittlement, resource.

1. Introduction

In 2021, the National Scientific Centre 'Kharkiv Institute of Physics and Technology' of the National Academy of Sciences of Ukraine (NSC 'KhIPT' NASU) together with the Argonne National Laboratory (ANL, USA) performed the physical start-up of a neutron source facility based on a subcritical assembly controlled by a linear electron accelerator (driver). In such electronuclear systems, the fission chain reaction is not self-sustaining and stops when the driver beam is turned off. The purpose of the development is to create a safe experimental base in Ukraine for neutron physics, materials science and medical research using intense neutron fluxes.

Primary neutrons are generated in photonuclear reactions by hard γ-radiation, which is formed during the scattering of electrons on the nuclei of heavy elements. The main components of the installation are as follows: a linear electron accelerator (100 MeV, 100 kW), a vacuum system for transporting the electron beam from the linear accelerator to the target, a neutron-generating target, and a subcritical assembly.

Based on thermohydraulic calculations of energy release and an acceptable level of energy density of the electron beam, a sectional design of the neutron-generating target was chosen: 7 plates with a thickness of 3 to 10 mm [1].

Two types of neutron-generating targets are being considered for use in future accelerator-driven safe nuclear power systems (ADS): liquid and solid metal. Among the latter, tungsten, tantalum, and alloys based on them attract the great attention of researchers.

Due to its high melting point, density and thermal conductivity, high compressive strength, and high neutron interaction cross-section, tungsten has been used as a target material in ADS systems such as LANCE and KENS for many years [2, 3]. However, tungsten corrodes in water, especially under irradiated conditions. This problem can be solved by coating the tungsten with a corrosion-resistant material. These include titanium, stainless steel, and tantalum.

Tantalum-coated tungsten targets have been used for decades in several ADS systems around the world (see Table 1).

Targets using tantalum–tungsten bimetal were used in the ISIS and KENS installations. A significant positive metallurgical factor is the good compatibility of these materials due to their complete solubility in the solid state.

One of the main requirements for this effective anticorrosion tantalum coating is to maintain reliable contact with the tungsten throughout the life of the target. The presence of a gap in the tungsten coating dramatically reduces the removal of heat from the target by means of a water stream. In turn, the tantalum coating leads to an improvement in the heat transfer of the target to the cooling water compared to tungsten.

Ensuring of a reliable Ta-tungsten contact, when creating a number of targets for megawatt Spallation Neutron Sources, is achieved due to the use of the hot isostatic pressing (HIP) method. The successful use of this method was first demonstrated at the ISIS facility (Rutherford Appleton Laboratory in Great Britain) [5] and then by Japanese scientists at the KENS facility [3].

For these purposes, a method of high-temperature vacuum rolling in combination with gas-phase deposition of tantalum on the side surfaces of the target has been developed at the NSC 'KhIPT' NASU. The scheme of

Table 1. **The principal characteristics of the ADS W–Ta targets**

Years	Country of the project	Beam parameters	Target concept	Ref.
1997–2020	USA, LANSE	48 kW, 0.06 mA, 800 MeV protons, pulse mode	W, water cooling	[2]
1980–2003	Japan, KENS	3 kW, 500 MeV protons, the world's 1st pulsating source for radiation materials science	W–Ta	[3]
2010	China, CSNS	120 kW of 1.6 GeV protons	A solid rotating target with W vessel — SS316, 10 mm	[4]
2010–2025	European Spallation Source (ESS), Lund, Sweden	2 GeV protons, 5 MW, 2.5 mA, rotating tungsten target	A solid rotating target with W 5400 hours per year	Launch — mid-2020s
1997–2018	ISIS, UK, Rutherford Appleton Laboratory	600 MeV protons, 160 kW	The first in the world W–Ta (target block) water cooling	[5]
2021	Ukraine, NSC 'KhIPT', ANL USA	100 MeV electrons, 1 mA, 625 Hz, 100 kW	Solid target U (Al), W (Ta)	Physical launch

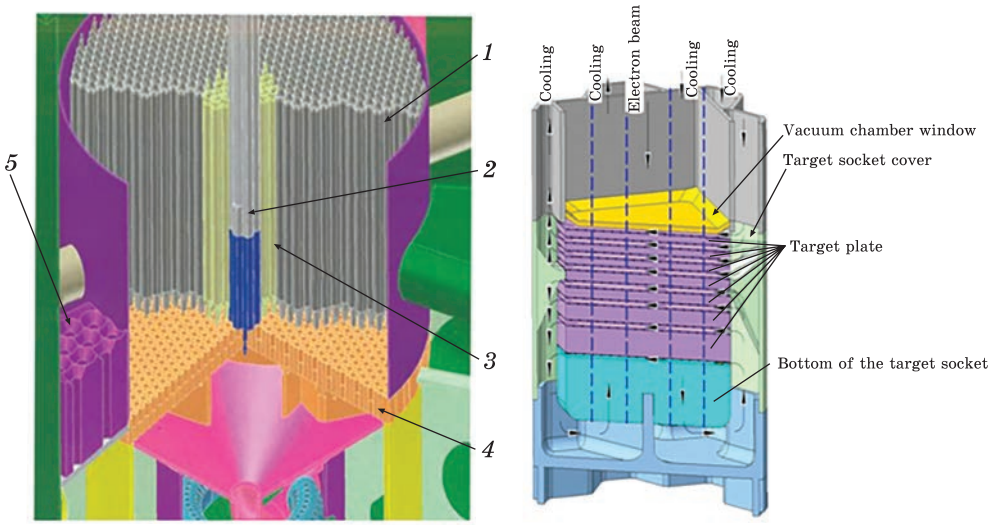

Fig. 1. (*a*) General view of the active zone of the subcritical assembly: *1* — graphite reflector; *2* — assembly of the neutron-generating target; *3* — fuel cells; *4* — lower grid for installing fuel assemblies and graphite reflector blocks; *5* — internal fuel storage box. (*b*) General view the tungsten neutron-generating target of the NSC 'KhIPT' NASU

the target, which is under a beam of electrons with energy of 100 MeV and is simultaneously irradiated by neutrons of a subcritical assembly, is presented in Fig. 1.

At the same time, pure tantalum with a thickness of 0.25 mm is used to the tungsten plates, as in the LANCE installation (USA). This value is determined by a compromise between ensuring, on the one hand, the reliability of tungsten protection against water corrosion in an active environment, and on the other hand, preventing a significant decrease in the neutron yield.

The disadvantages of tantalum as a target material can be considered a relatively large cross-section of interaction with neutrons (especially in the epithermal energy range), which leads to its high radioactivity after irradiation. A calculation made for the European Spallation Source (ESS) installation (5 MW) showed that after a year of exposure, tantalum would have an indicated activity ten times greater than tungsten or mercury. It is because of this that two nuclear installations — KENS and ISIS — at one time changed tantalum targets to pure tungsten.

2. Degradation of the Mechanical Properties of Ta, W, and Their Alloys

Tungsten and other elements of the group VI of Periodic table (for example, chromium) in the absence of irradiation demonstrate a significant tendency to lose plasticity, which is connected with the features of the

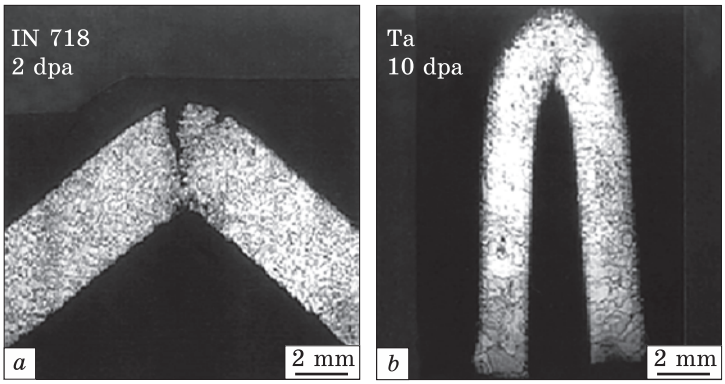

Fig. 2. Bending tests of irradiated samples of high-nickel alloy Inconel 718 and pure tantalum. A huge margin of plasticity of tantalum irradiated to a dose of 10 dpa (displacement per atom) compared to a high-nickel alloy is shown [2]

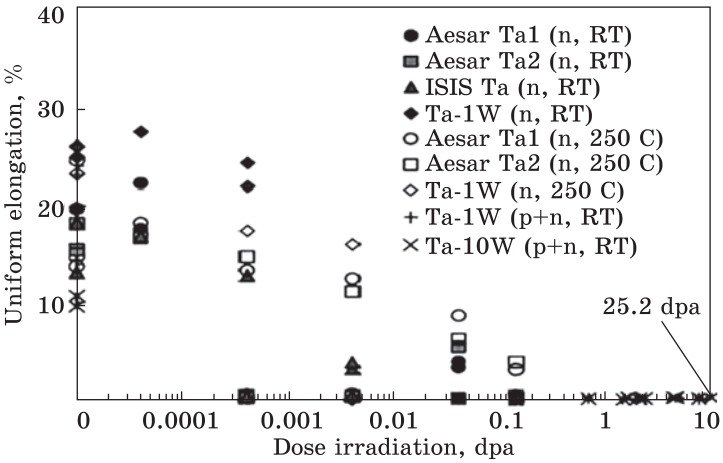

Fig. 3. Dose dependence of uniform elongation of tantalum and its alloys irradiated with neutrons and protons [3]

electronic structure of these metals. Unlike tungsten, tantalum does not show a tendency to brittleness without irradiation. Its mechanical properties under irradiation are poorly studied and controversial. Thus, work [6] revealed high plasticity of tantalum irradiated to a dose of 10 dpa (Fig. 2).

At the same time, at doses of 10^{-4} dpa, during irradiation at the LANCE neutron source (800 MeV protons, 1 mA current, irradiation temperature of 50–160 °C), its plasticity at room temperature also begins to decrease (from 32 to 27%), and, at a dose of about 0.14 dpa, Ta completely lost its initial high plasticity (Fig. 3) [7].

It is important to note that the difficulty of forecasting the 'survivability' of the W–Ta target is also connected with the fact that, with the exception of the work carried out at the NSC 'KhIPT' NASU in 70–90s of the last century (see, *e.g.*, Ref. [8]), in the world there are no experimental works on radiation damage of reactor materials by high-energy electrons with an energy of 100 MeV and above.

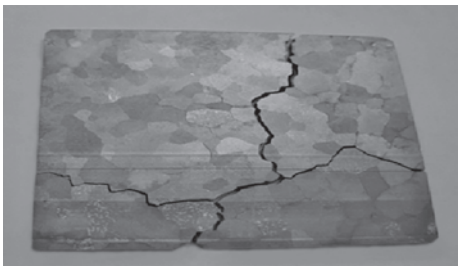

Fig. 4. Recrystallization embrittlement of cast tungsten. The material collapsed during manual operation

It is interesting to compare the one presented in Fig. 3 dose dependence of the loss of plasticity of tantalum and its alloys irradiated with neutrons and protons, with the behaviour of a number of reactor materials irradiated with high-energy electrons with an energy of more than 100 MeV at the NSC 'KhIPT' accelerators LPE 300 and LP 2 GeV, that is, in conditions close to the operation of the target of the KhIPT neutron source. The comparison shows that the threshold dose for the onset of plasticity reduction in both cases is practically the same and is about 2–3 10^{-4} dpa [9].

Unlike materials with an f.c.c. type of crystal structure, many b.c.c. metals, especially, metals of groups V, VI of the Periodic table of elements, which include tantalum and tungsten, can exhibit brittleness and a complete loss of fracture toughness and in un-irradiated state. This primarily concerns the so-called 'recrystallization' embrittlement of tungsten, which occurs as a result of high-temperature annealing of the cast material, which was previously subjected to thermomechanical processing, for example, after annealing rolled tungsten (Fig. 4).

Such effects gave reason to change the direction of research in the direction of powdered tungsten. However, it turned out that the brittle–viscous transition temperature T_x of this material even in the unirradiated state is 180–230 °C [10]. As a result, we have a situation where even before the irradiation process begins; the material is already in a fragile state. In this case, it is necessary to use the value of the temperature shift of the brittle–viscous transition, ΔT_x, to assess the influence of irradiation.

During the study of the influence of neutron irradiation on the brittleness of tungsten and the highly plastic alloy W–10% Re, it was established that T_x increases by 200 °C already at a dose of 0.4 dpa. At the same time, already at doses of 0.1–0.2 dpa, the shift of T_x is hundreds of degrees [11] (Fig. 5).

Its sharp decrease with increasing irradiation temperature is observed, which is typical, when conducting mechanical tests of irradiated b.c.c. materials [12]. Thus, target-operating temperatures of 100 °C are the most dangerous from the point of view of radiation embrittlement.

It is important to note that the W–Re alloy has no advantage in the rate of radiation embrittlement. The reason is the build-up of nuclear reaction products and, as a result, the formation of radiation-induced precipitates (χ-phase Re_3W) [13] even at low doses of exposure.

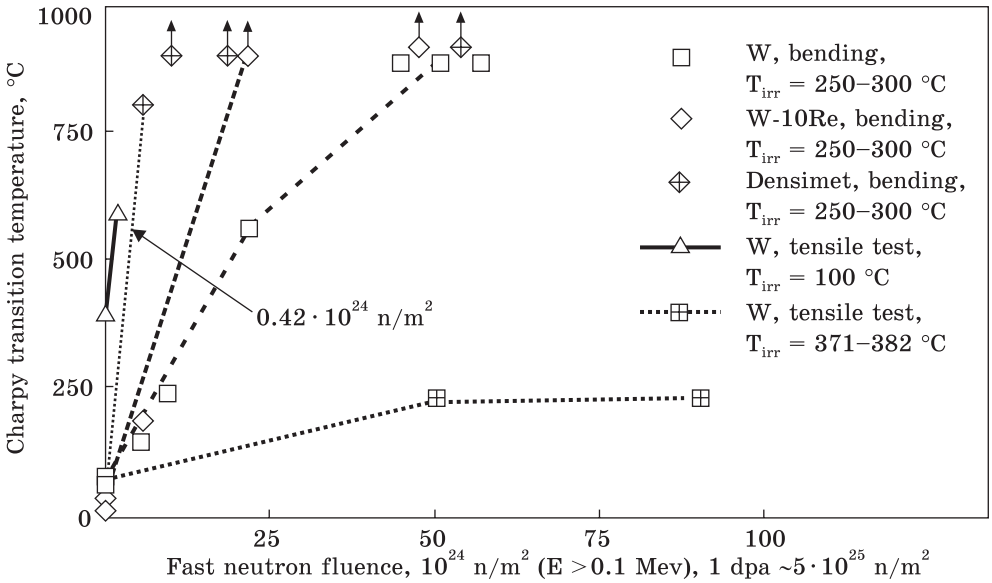

Fig. 5. Dose dependence of the brittle–viscous transition temperature for tungsten and its alloys [11]

However, this is not only that. The results of structural studies show that a feature of radiation damage to tungsten and its alloys, compared to f.c.c. metals and steels, is a very low temperature and dose threshold for the onset of radiation porosity (less than $0.2T_m$ and 0.15 dpa, respectively) [13].

One of the crucial conditions for the reliable operation of the target is the understanding of the type and number of radiation defects formed under the operating conditions of the target of the NSC 'KhIPT' NASU neutron source. A recent work [14] provided significant help in this. It showed that at irradiation temperatures of the order of 100 °C and doses that do not exceed a few dpa, the main type of defects are dislocation loops (Fig. 6).

The use of single crystals does not 'save' the situation. Thus, already at a dose of 1.67 dpa, in the most 'soft' test conditions (for a 4-point bend), the shift T of pure tungsten amounted to more than 500 K [15].

It should be noted that all the above-mentioned regularities of the effect of irradiation on the ductile–brit-

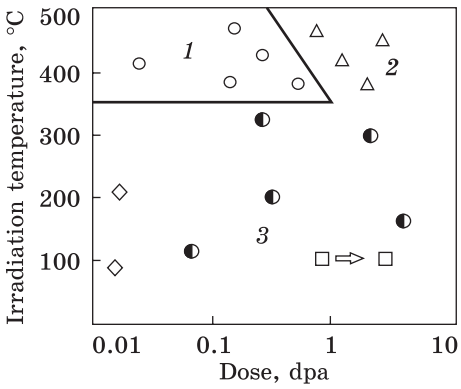

Fig. 6. Areas of existence of various defects in tungsten: *1* — pores and loops; *2* — pores and discharge; *3* — dislocation loops [14]. Squares and an arrow indicate the operating conditions of the NSC 'KhIPT' tungsten target for 3 years of operation

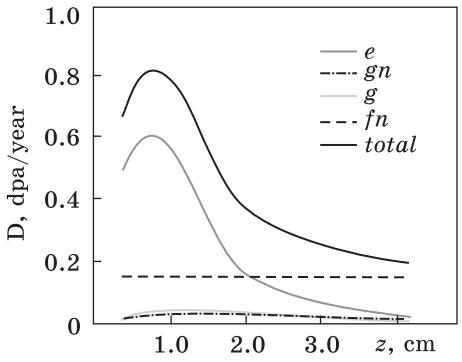

Fig. 7. Total rate of defect formation in tungsten [15]. Here, *e* denotes an elastic scattering of electrons, *gn* — scattering of photoneutrons on nuclei, *g* — formation of recoil nuclei during (*g*, *n*) reactions, *fn* — scattering of neutrons

tle transition temperature (DBTT), namely its increase, shift towards higher temperatures due to the action of irradiation, are typical for irradiated by various types of particles of materials with b.c.c.-type crystal structure.

3. Assessment of the Level of Radiation Damage of the Target

Radiation damage to the targets of ADS installations has significant differences from damage in conventional fission reactors. This applies to the two main components of damage, namely, defect accumulation rates and transmutation gases. Thus, it was established that two-thirds of all damage to the Spallation Neutron Source of the Oak Ridge National Laboratory (USA) is caused by high-energy spallation neutrons, while the rate of gas accumulation during irradiation with high-energy protons (with energy of the order of GeV) is an order of magnitude higher, than during irradiation in fission reactors and thermonuclear reactors [16].

The tungsten target of the Neutron Sources of the NSC 'KhIPT' NASU has already worked under a beam of high-energy electrons with energy of 100 MeV in the process of setting up the accelerator and physical start-up of the installation in total for more than a year. Therefore, the question of its radiation damage is relevant. For this, mathematical modelling was carried out using the MCNPX program of the set of processes occurring in the tungsten target during irradiation [17].

Figure 7 shows the total rate of defect formation in tungsten and the partial contributions of various mechanisms of radiation damage, where *e* — elastic scattering of electrons, *gn* — scattering of photoneutrons on nuclei, *g* — formation of recoil nuclei during (γ, *n*) reactions, *fn* — scattering of neutrons, that came out of the subcritical assembly, on the cores of the target.

The maximum sleep dose rate/year is reached in the second plate of the tungsten target (at a depth of $\gg$1 cm; see Fig. 7) and is associated with the elastic scattering of high-energy electrons. This value is two orders of magnitude lower than the dose rate expected in a uranium target under the same irradiation parameters [18].

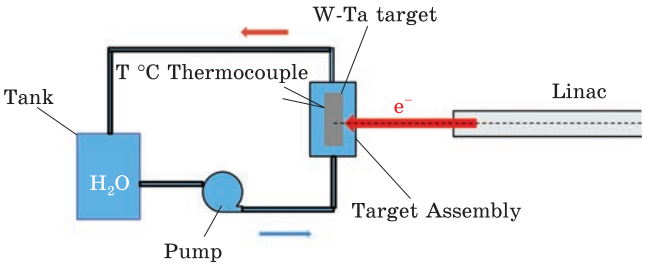

Fig. 8. Scheme of irradiation of the target tungsten–tantalum plate (accelerator KUT-30, electrons of 6.5 MeV, current of 60 μA; 60 h, electron flow density of 65 μA/cm², fluence of $2 \cdot 10^{20}$ electrons/cm²)

As shown in Refs. [4, 19, 20], the resource of tungsten targets of the Chinese neutron source CSNS (protons 1.6 GeV, 120 kW) and the European neutron source ESS (protons 2 GeV, 5 MW) is 4–5 years of continuous operation, which corresponds to approximately the radiation doses, approximately 10 dpa.

4. Control of the Tightness and Coating on the Target Plates by the Method of Sampling the Cooling Water during Irradiation with Electrons

The study of the tightness of the Ta–W–Ta target was carried out with the help of a Shimadzu plasma spectrometer by analyzing samples of cooling water during the irradiation of Ta–W–Ta samples on the KUT-30 accelerator with electrons with energy of 6.5 MeV, at a current of 60 μA, for duration of 60 h. The density of electron flow was of 65 μA/cm², the fluence was of $2 \cdot 10^{20}$ electrons/cm² (Fig. 8).

The sample was cooled with distilled water in a closed circuit. Therefore, seven water samples were selected for elemental analysis: sample #1 — the first intake of water before irradiation; sample #2 — after 12 h of irradiation; sample #3 — after 22 h of exposure; sample #4 — after 32 h of exposure; sample #5 — after 32 h of exposure; sample #6 — after 42 h of exposure; sample #7 — after 60 h of exposure. Table 2 shows the data of the elemental analysis of 7 water samples (samples Nos. 1–7), obtained using the Shimazu plasma spectrometer.

Table 2. **Results of measuring tungsten content in cooling water**

Classification of the sample	Sample No.	*G*	*W* (quant average), mg/l	*W* (wave length)
UNK	1	1	–0.0458	207.911 (1)
UNK	2	1	–0.0367	207.911 (1)
UNK	3	1	–0.0456	207.911 (1)
UNK	4	1	–0.0509	207.911 (1)
UNK	5	1	–0.0390	207.911 (1)
UNK	6	1	–0.0358	207.911 (1)
UNK	7	1	–0.0397	207.911 (1)

As a result of the inspection, the following was established: a tantalum thickness of 250 μm provides a sufficient barrier against the entry of tungsten into the cooling water when irradiated with electrons with a flux density of 65 μA/cm^2 and a fluence of 2×10^{20} electrons/cm^2.

5. Occurrence of Stresses during Target Irradiation

Assuming that the main source of stresses is the occurrence of thermoacoustic macrostresses, let us consider what stresses can arise in a tungsten target under the action of a beam of high-energy electrons with an energy of 100 MeV, a beam power of 100 kW and an electron beam power density on the target of 2 kW/cm^2, which corresponds to the operating conditions of a neutron sources.

The stress level in tungsten metal plates can be estimated using the expression [21]:

$$\sigma \propto \Gamma J \rho \chi;$$

here, Γ is the Grüneisen parameter; χ is the specific loss of the beam in the target, which can be approximated with a sufficient degree of accuracy by the expression

$$\chi = a\rho$$

with a — specific ionization loss, ρ — material density; J — the so-called electronic fluence per pulse calculated by the formula

$$J = W/\pi R^2 f E,$$

where W is the power of the beam equal to 10^5 watts, R is the radius of the electron beam (2.5 cm), f = 100 Hz, E = 100 MeV. The calculations performed for the parameters: Γ = 1.6, the density of the target material is of the order of $\rho \approx 19$ g/cm^3, and ≈2 MeV/cm^2, $J = 3\cdot10^{12}$ electron/cm^2 showed that the level of the most dangerous tensile thermoacoustic stresses in the targets is approximately 31 MPa [21]. The authors of this work showed that increasing the frequency of irradiation pulses (up to 600 Hz as expected) would not lead to an increase in the stress level in the irradiated material.

6. Analysis of Hardness and Nanohardness of the Target Material

Figure 9 presents a graph of the Vickers hardness dependence of the NSC 'KhIPT' composite target and the Japanese ADS Spallation target KENS [3] of the same composition: Ta (upper layer 250 μm)–Ti (intermediate layer of the order of 60 μm)–powder W (main volume target).

It can be seen that there is a good correspondence between the hardness values of all components of the target, despite the fact that the connection of W with Ta in work [3] was carried out using the method of hot isostatic pressing at temperatures of 1400–1500 °C, and the KhIPT target was fabricated using the method of high-temperature vacuum rolling at temperature of 1300 °C.

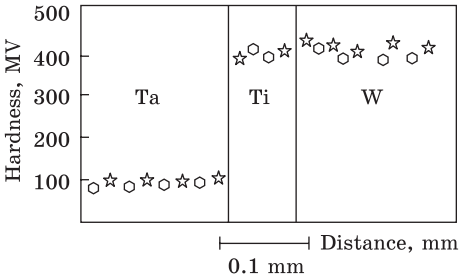

Fig. 9. Comparative hardness distribution by target depth for targets of KENS [3] and NSC 'KhIPT'

The same effect at the tantalum–titanium interface is also observed during the analysis of the nanohardness distribution on the G200 (USA) device (Fig. 10).

Two points should be noted. The first is a sharp increase in the nanohardness of tantalum, when approaching the interface. The second is the formation of a maximum in the boundary regions of titanium. As recently shown [22], the first effect is determined by mass transfer (in this case of titanium) through the interface with the help of dislocations and disclinations. The second is due to the increased density of dislocations (the formation of so-called 'roofs' due to pile-up processes) in the grain boundary regions, compared to the body of the grain.

Figure 11 shows the structure of the titanium interlayer W–Ti–Ta of the target, which indicates a high degree of rolling (the presence of slip bands) and complete filling of the microuniformities of the tungsten interface (×500) during the formation of titanium–tungsten contact.

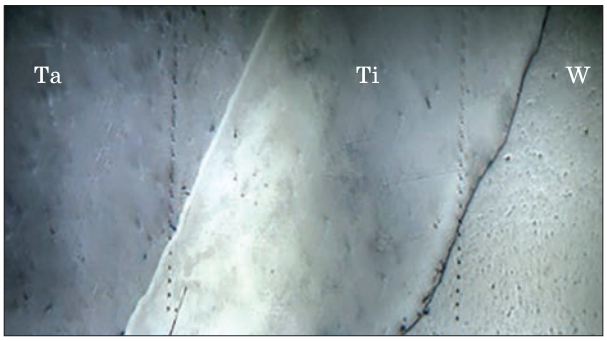

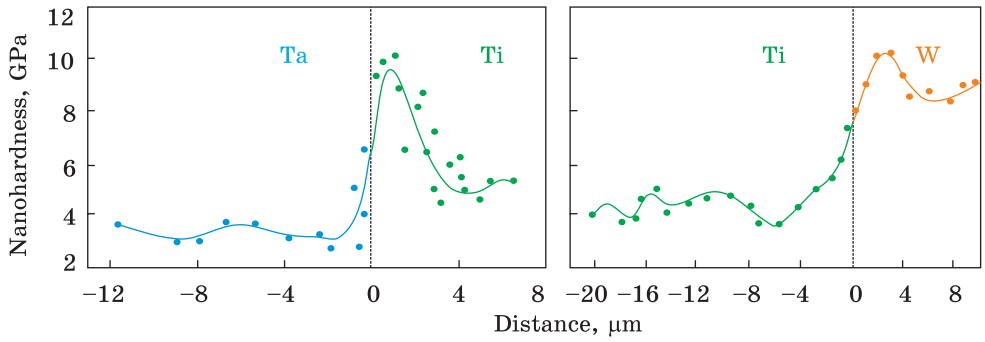

Fig. 10. Nanohardness distribution across the tantalum–titanium interface (shown as '0' in the graphs below)

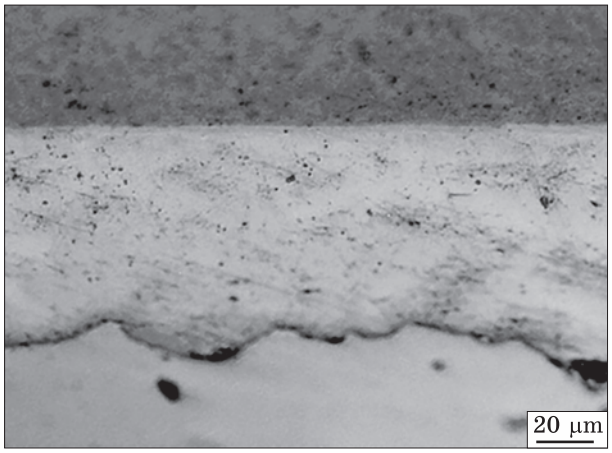

Fig. 11. Structure of the deformed titanium layer of the W–Ti–Ta target: tantalum on top, titanium in the middle, tungsten on the bottom) (×500)

7. Mechanical Properties of Tantalum

This section focuses on the results of studies of samples corresponding to different stages of target preparation.

No. 1. Tantalum samples (in delivery condition) in the form of rolled foil with a thickness of 0.5 mm (purity 99.8%). Shown in Fig. 12 tantalum has a fibrous microstructure, which is characteristic of a deformed metal. Apparently, the tantalum strip was subjected to high-temperature heating with subsequent deformation. The microhardness of the studied tantalum varies from 170 kg/mm^2 to 220 kg/mm^2 with an average value of 195 kg/mm^2.

No. 2. Tantalum rolled samples annealed at 1300 °C. After etching on the grain structure, mostly equiaxed grains with an average size of 350 μm were found on the annealed tantalum rolled sample (Fig. 13). The microhardness of such tantalum was 140–145 kg/mm^2 according to *HV* [25].

No. 3. Tantalum obtained by the CVD method. Tantalum obtained by chemical vapour deposition (CVD) by the thermal dissociation reaction of $TaCl_5 \leftrightarrow$ Ta (solid) + 5Cl (gas) on a graphite base at a temperature of 1600°C was used for research, and for comparison, annealed tantalum ribbons obtained by rolling. After removing the graphite base from CVD Ta, samples were cut for metallographic studies and tensile tests. After etching, a fine-grained structure with an average size of 50 μm was found on the samples obtained by the CVD method (Fig. 14).

The microhardness of CVD tantalum was 145–160 kg/mm^2 according to *HV* [25]. The boundaries of the grains in both cases are thin, mostly without impurity precipitates, and in the middle of the grains, there is a pronounced intragranular structure in the form of pits of etching along the entire field of the section, decorated with impurity atoms on the defects of the crystal lattice.

Tensile tests were performed on all types of samples. The moving speed of the mobile gripper was 2 mm/min. The test results are given in Table 3.

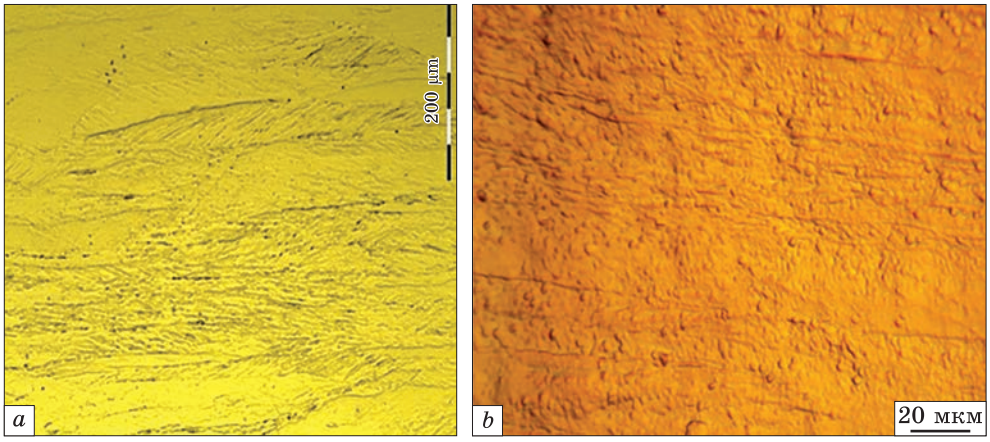

Fig. 12. Structure of the obtained tantalum (#1): *a* — ×200; *b* — ×1500

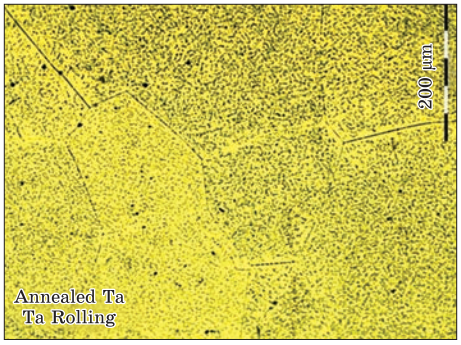

Fig. 13. Structure of annealed tantalum

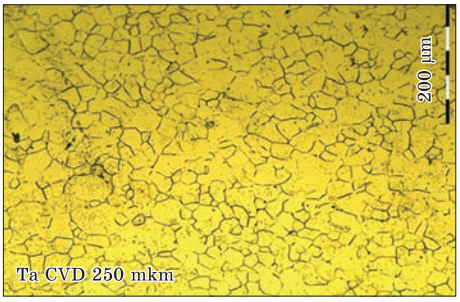

Fig. 14. Photomicrographs of CVD Ta samples after etching

As follows from the comparison of the obtained results, the average value of the strength σ_b of CVD tantalum is 29% lower than the average value of the annealed Ta; the yield strength $\sigma_{0.2}$ is lower by 35% than the values of the yield strength of the annealed specimens Ta and the average value of elongation δ is lower by 43%.

Table 3. **Tensile test results (room temperature)**

	σ_b, MPa	σ_{02}, MPa	δ, %
Annealed Ta			
Average	335	278	28
CVD deposited Ta			
Average	237	182	16
Unannealed strip			
Average	578	476	5.9
Annealed strip rolled to 250 mm			
Average	600	170	1.45

The results of tensile tests at 20 °C for samples cut from tantalum strip 0.5×90×500 mm perpendicular to the rolling direction show that the material has low relative-elongation values not exceeding 6%, and samples rolled at room temperature to the required coating thickness of 259 μm have the lowest plasticity values.

8. Main Mechanisms of Target Destruction

As shown by the elemental analysis of the fracture surface using the ELVAX analyser, the concentration of iron on the grain boundaries is an order of magnitude higher than its content in the matrix and is about 0.3–0.5 percent. Considering the low solubility of iron in tungsten, W–Fe intermetallics can make a significant contribution to the process of grain-boundaries' destruction, but not only them. In metals of the VIth period of the Periodic table of the elements, which includes tungsten, penetration impurities are highly active in relation to grain boundaries. This is due to the high bond energy of such elements as carbon, oxygen, as well as sulphur and phosphorus. Moreover, the bond energy value increases when going from chromium to tungsten.

As shown by the studies carried out in Ref. [23], in tungsten and molybdenum due to the segregation phenomenon, grain boundaries are almost completely filled even at a carbon concentration of 0.1%. This can occur due to the 'Robbins mechanism' associated with the establishment of covalent resonance bonds in defective places of the crystal structure, which are grain boundaries [24].

As established in the work carried out at the I.M. Frantsevych Institute for Problems in Materials Science of the N.A.S. of Ukraine, the properties of transition metals largely depend on the so-called parameter DLVE (the degree of localization of valence electrons), which determines the contribution of the covalent component to the binding energy of metals [25]. In heat-resistant b.c.c. metals, it is more than 80%. In turn, the connection between the covalence of materials and their fragility is a well-established fact [26, 27].

The use of Mössbauer spectroscopy to analyse the behaviour of a number of transition metals irradiated with high-energy electrons with an energy of more than 100 MeV at the accelerators of the KhIPT LPE 300 and LP 2 GeV made it possible to establish that the degree of low-temperature radiation embrittlement of metallic materials increases with an increase in the number of localized electrons (electrons that can participate in covalent directional bonds). This gave reason to assert that at all structural levels considered, including the intraatomic, electronic level, radiation damage is associated with the manifestation of the effect of structural localization [28].

9. Testing for Three-Point Bending of W–Ti–Ta Plates Made of Powdered Tungsten

Unlike materials with an f.c.c. crystal structure, many b.c.c. metals, including tungsten, can exhibit brittleness and a complete loss of fracture toughness even in the un-irradiated state. For example, in Ref. [29], the results of tests on the impact strength of Charpy-type samples of different

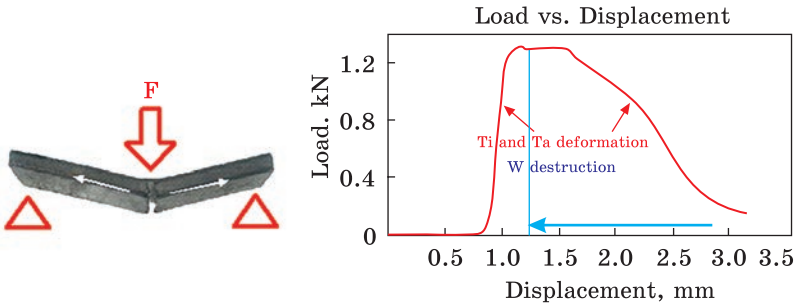

Fig. 15. The result of tests on three-point bending at 20 °C [30]

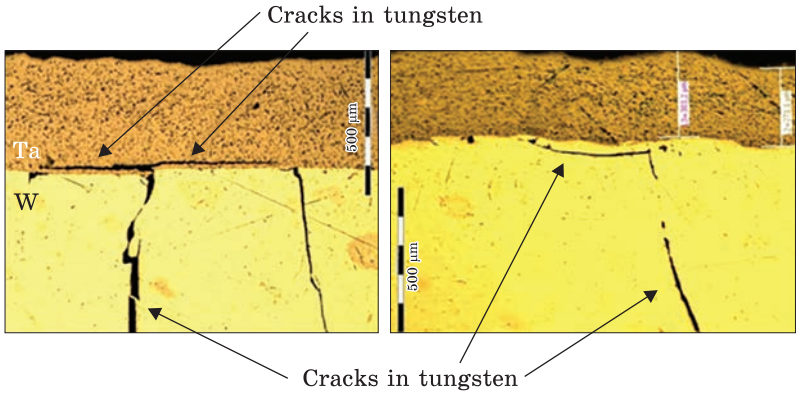

Fig. 16. Metallographic images of tantalum coated tungsten specimens after three-point bending tests near (≈2 mm) the fracture zone [30]

geometries are given. They show that pure tungsten remains brittle even in the unirradiated state up to a temperature of 600 K.

Considering this, the 3-point bending method is used to analyse the mechanical characteristics of brittle materials, and in particular, the metal of tungsten–tantalum targets. In our work, such tests were carried out in accordance with the requirements of the ASTM E855-90 standard.

The fundamental difference in the nature of the destruction of such multilayer connections compared to monometallic tungsten is the presence of a plastic deformation region before the destruction of tungsten already at room temperature, which appears due to the deformation of the clad layers of tantalum and titanium, which in the conditions of three-point bending work to break (Fig. 15).

Figure 16 shows micrographs of the deposited tantalum layer on destroyed samples. Metallographic studies show that the destruction does not occur along the Ta–W junction, but along tungsten or tantalum. In tantalum and tungsten, there are defects in the form of cracks that de-

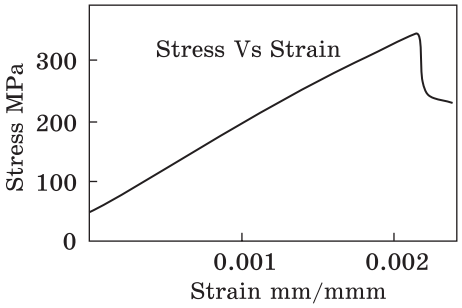

Fig. 17. Load stress (MPa)–strain (mm/mm) curve for W–Ti–Ta plate at room temperature (span — 47 mm, rate — 0.8 mm/min, width — 6 mm)

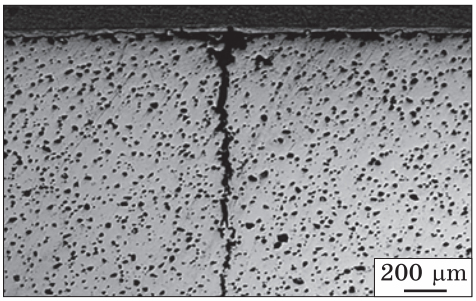

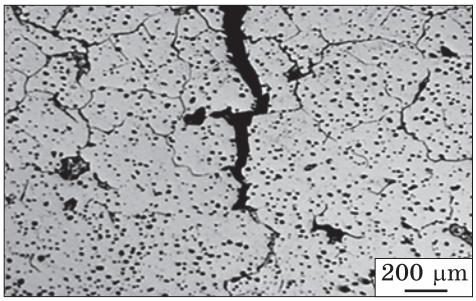

Fig. 18. General cross-section of a target plate with a brittle, propagating crack

Fig. 19. The initiation of brittle cracks at the boundaries of tungsten grains

velop both longitudinally and transversely relative to the joint boundary. Some of them go beyond the layer and spread into the plate of the opposite material. However, the absence of destruction of the very boundary of the tantalum–tungsten connection indicates that its strength remains higher than the strength of each of the components.

Figure 17 shows the load curve of a 3 mm target plate versus the amount of bending deformation. Plastic deformation of the plate is practically absent (0.22%), and the magnitude of the destructive stress is more than 300 MPa, which significantly exceeds the calculated values of the thermoacoustic stresses given above. At the same time, as can be seen from Fig. 17, complete unloading of the sample is not observed. The analysis of the structure of the destroyed composite showed that the brittle crack that propagates does not 'penetrate' the tantalum coating, and the sample remains 'hanging' on it (Fig. 18).

A crack initiated by a stress of more than 300 MPa has passed through tungsten and titanium, unable to 'penetrate' the tantalum coating (top of image).

Structural analysis showed that in powdered tungsten, as well as in cast, crack initiation occurs at grain boundaries (Fig. 19).

10. Effect of the Amount of Rolling Deformation on the Adhesive Strength of the Coating

The adhesion strength of the coating was determined during peel tests of the plated layer (Fig. 20) [30]. The tests were carried out on the Bi-00-201 Nano servohydraulic testing machine. Samples for testing were cut by the electric spark method on a ZAPbp BP-96ds machine. The quality of the joint zones of the samples was assessed by metallographic studies using an optical microscope of the LECO Company. Electron-probe x-ray spectral research was performed using a Quanta 200 3D ion–electron microscope.

When the amount of deformation during rolling is of 1.5–1.6%, the joint area of compatible deformed materials is 75–80% (Fig. 2, *a*). Strength spikes during mechanical tests for separation of the clad layer (Fig. 21, *a*) also indicate the local nature of the solid-phase connection of the layers. The average strength of the connection of the layers was 10 N/mm, which corresponds to the peak strength value, when rolling these materials without interlayers. The minimum strength of 7 N/mm corresponds approximately to the average strength value, when rolling tungsten with tantalum without inter layers.

An increase in the relative compression composite to 3.2% ensures a complete fit of the layers. Metallography of the zones of W–Ti and Ti–Ta joints proved the absence of defects in the form of pores, delaminations, cracks (Fig. 21, *b*). The adhesion strength of the clad layers for separation is 13 N/mm. The strength graph has no obvious spikes. This can be explained by the uniform fit of the layers along the entire border of the layer connection, which corresponds to 100% of the area of the layer connection.

A further increase in the relative compression causes an increase in the strength of the layer connection up to 15 N/mm due to strain hardening of the materials that make up the solid-phase connection.

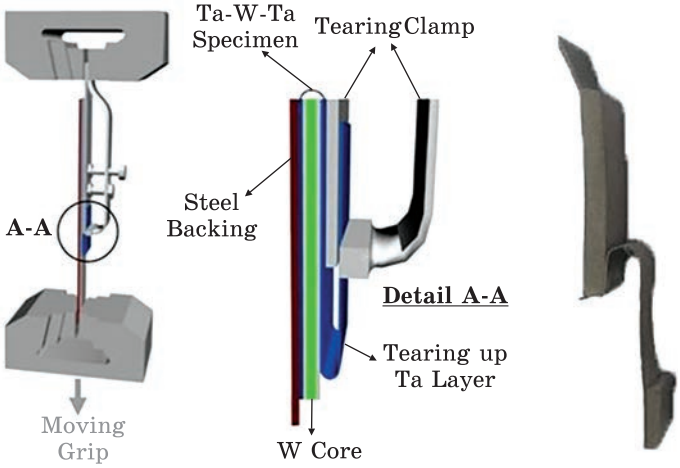

Fig. 20. (*a*) Schematic of tear strength tests of tantalum coating on tungsten. (*b*) Appearance of the sample after testing [30]

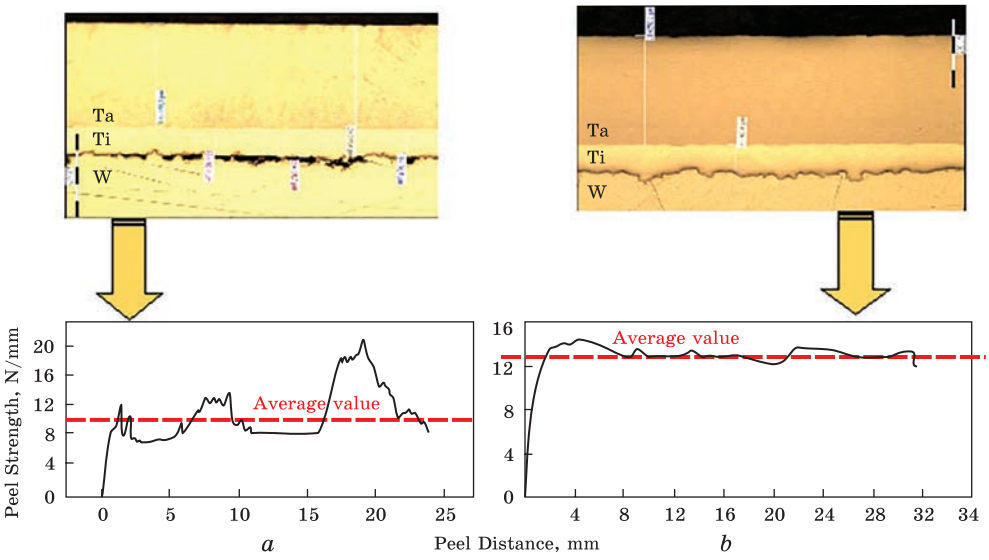

Fig. 21. Microstructure and 'breakaway' test curves of Ta–Ti–W–Ti–Ta samples under conditions of different degrees of deformation [30]. Here, (*a*) T = 1300 °C, ε = 1.6% (ΔH = 0.05 mm, H_{end} = 3.0 mm); (*b*) T = 1300 °C, ε = 3.2% (ΔH = 0.1 mm, H_{end} = 3.0 mm)

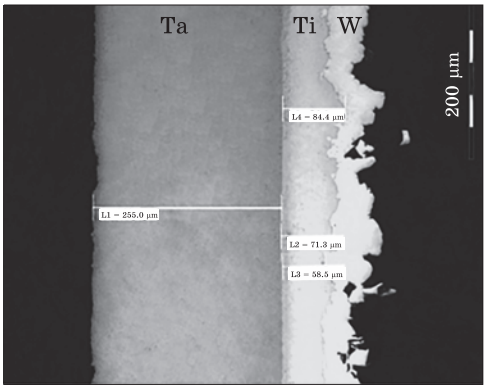

At. number	Element	Concentration, %
22	Ti	0.2515±0.0162 %
23	V	0.0282±0.0046
26	Fe	0.0321±0.0026
28	Ni	0.0167±0.0015
73	Ta	0.6933±0.0152
74	W	97.9190±0.0258
75	Re	1.0593±0.0127

Fig. 22. Microstructure and x-ray fluorescence analysis of the detachment surface of the plating layer [30]

Exceeding the compression above 6–7% led to distortion of the entire solid-phase connection as a whole. Samples of multilayer materials required additional mechanical processing and straightening, which is not always possible in the case of a tungsten core.

Studies have shown that the detachment of the plating layer of the solid-phase connection occurs along tungsten that is confirmed by both metallographic and x-ray fluorescence analysis (Fig. 22).

Moreover, the destruction of the samples occurred at a distance of no less than 30–50 μm from the joint boundary. This testifies to the high

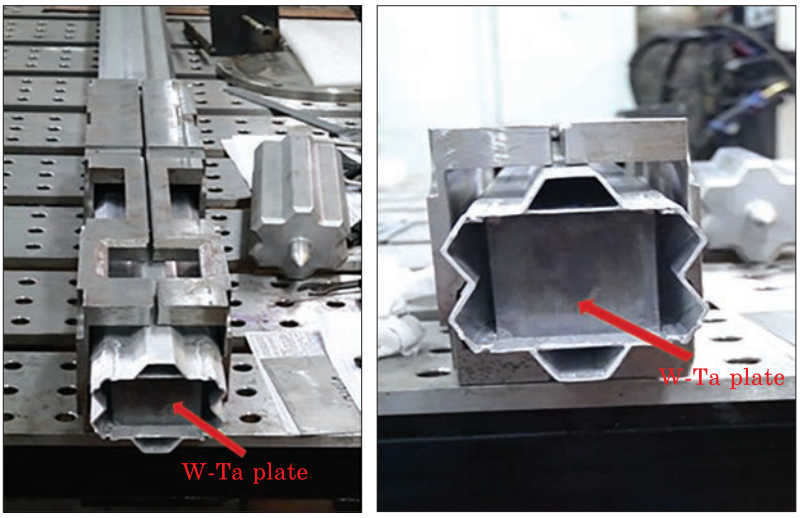

Fig. 23. Installation of tungsten targets in the housing of the SAV-1 aluminium-alloy accelerator ion channel. The general view of the location of the ion conductor with the target in the active zone of the subcritical assembly was presented in Fig. 1, *a*

strength of the connection between the Ta and W layers through the Ti layer and a fairly wide connection boundary, which makes 3% the optimal threshold compression for Ta–W–Ta samples (with Ti interlayers).

The physical foundations of the nanomechanism of bonding in the solid phase of tungsten and tantalum at the dynamic and isostatic stages at hot vacuum pressing are formulated. Experimental data on the relative temperature convergence of rolls at the dynamic and isostatic stages of hot vacuum pressing have been obtained [31].

After manufacturing a complete set of targets consisting of seven Ta–Ti–W–Ti–Ta target plates (Fig. 23), the entire set of plates was placed in a housing made of SAV-1 aluminium alloy and welded by argon-arc welding method TIG. After that, acceptance tests of the neutron-generating target of the Neutron Source were conducted.

Conclusions

A retrospective review of the results of experimental and theoretical studies of the properties of both the component metals of the plates and the composite W–Ti–Ta neutron-generating target of the neutron source of the NSC ‘KhIPT’ is given.

(i) Mathematical modelling was carried out using the MCNPX program of the complex of processes occurring in the tungsten target during irradiation. It was established that the maximum damage rate 0.83 dpa/year is achieved in the second plate of the tungsten target (at a depth of ≈1 cm) and is associated with the elastic scattering of high-energy electrons.

(ii) Using the method of water sampling, which cools the target plates irradiated with high-energy electrons, control was carried out and the tightness and coating of the target was established.

(iii) Considering that the main source of stress is the occurrence of thermoacoustic macrostresses in the target plates under the action of a beam of 100 MeV electrons, an assessment of their magnitude in the tungsten target was carried out. It was determined that it can be of the order of 30 MPa, which is significantly lower than the level of destructive stresses during bending and tensile deformations of the target plates.

(iv) An analysis of the distribution of hardness and nanohardness across the tantalum–titanium–tungsten interface was carried out. It was established that the lowest values of these values are observed in tantalum (about 100 *HV*), while in titanium and tungsten they are at the level of 370–400 *HV*. The high values of the hardness of the titanium layers can be explained by the effect of a sharp increase in strength (according to the hyperbolic dependence) and hardness of the layer during high-temperature rolling when its thickness is reduced to values less than 0.1 mm.

(v) An analysis of the results of the mechanical properties of tantalum at various stages of target preparation was carried out:

- in the condition of delivery (in the form of a 0.5 mm thick strip);
- after high-temperature annealing of rolled products;
- samples made from an annealed strip rolled to 250 μm;
- from tantalum obtained by the gas-phase deposition method (CVD Ta).

At the same time, the lowest values of plasticity (1.5%) and the highest values of strength (up to 600 MPa) have the annealed samples rolled 'cold' to the required coating thickness of 250 μm.

(vi) The mechanisms of destruction of target plates made of cast and powdered tungsten were studied. As established, the grain boundary character of the destruction is a general regularity. Physical mechanisms explaining this behaviour of the metal are proposed.

(vii) Using the 3-point bending method, in accordance with the requirements of the ASTM E855-90 standard, bending deformations of the target plates were carried out. It was found that the plastic deformation of the plates is practically absent (about 0.22%), and the value of the destructive stress is more than 300 MPa, which significantly exceeds the calculated values of the thermoacoustic stresses that occur in targets under irradiation with high-energy electrons.

(viii) An analysis of the cohesive strength of the adhesion of the tantalum coating to the surface of the tungsten plates of the target using the peel method (for separation) was carried out. It is shown that the titanium interlayer leads to a two-fold increase in the pull-off force (cohesive strength of the coating).

(ix) The optimal parameters of the degree of deformation during high-temperature vacuum rolling to create a high-quality Ta–Ti–W connection

were determined. It was established that the degree of deformation at the level of 3% is the optimal value during high-temperature vacuum rolling to create a high-quality Ta–Ti–W connection of the target components.

(x) As a result of the performed work, a complete set of Ta–Ti–W plates of the neutron-generating target Neutron Source was produced, which was placed in an aluminium case made of SAV-1 aluminium alloy. The target has already worked under a beam of high-energy electrons with energy of 100 MeV in the process of setup and physical launch for more than a year.

Acknowledgements. This work was carried out thanks to the support of the International Scientific and Technical Center of Ukraine, the Argonne National Laboratory, and the US Department of Energy. Personal thanks to Y. Gohar, I. Bolshynskyi, and Member of the N.A.S. of Ukraine I.M. Neklyudov (NSC 'KhIPT' NASU).

REFERENCES

1. I.M. Karnaukhov and A.Yu. Zelinsky, *Problems of Atomic Science and Technology*, No. 3 (133): 3 (2021). https://doi.org/10.46813/2021-133-003
2. M.S. Wecsler, J. Sommer, C. Lin, L.L. Daemen, and P.D. Ferguson, *J. Nuclear Mater.*, **244**, No. 3: 177 (1997). https://doi.org/10.1016/S0022-3115(96)00735-0
3. M. Kawai, M.M. Kawai, M. Furusaka, K. Kikuchi, H. Kurishita, R. Watanabe, J.-F. Li, K. Sugimoto, T. Yamamura, Y. Hiraoka, K. Abe, A. Hasegawa, M. Yoshiie, H. Takenaka, K. Mishima, Y. Kiyanagi, T. Tanabe, N. Yoshida, and T. Igarashi, *J. Nuclear Mater.*, **318**: 38 (2003). https://doi.org/10.1016/S0022-3115(03)00114-4
4. W. Yin, Q.Z. Yu, Y.L. Lu, S.L. Wang, J.F. Tong, and T.J. Liang, *Journal Nuclear Materials*, **431**, Nos. 1–3: 39 (2012). https://doi.org/10.1016/j.jnucmat.2011.11.025
5. D. Wilcox, P. Loveridge, T. Davenne, L. Jones, and D. Jenkins, *J. Nuclear Mater.*, **506**: 76 (2018). https://doi.org/10.1016/j.jnucmat.2017.10.075
6. J. Chen, P. Jung, M. Rödig, H. Ullmaier,and G.S. Bauer, *J. Nuclear Mater.*, **343**, Nos. 1–3: 227 (2005). https://doi.org/10.1016/j.jnucmat.2004.09.076
7. T.S. Byun and S. Maloy, *J. Nuclear Mater.*, **377**, No. 1: 72 (2008). https://doi.org/10.1016/j.jnucmat.2008.02.034
8. V.F. Zelenskij, I.M. Neklyudov, L.S. Ozhigov, V.V. Gann, A.A. Parkhomenko, B.V. Borts, and V.F. Stefanov, *J. Nuclear Mater.*, **207**: 280 (1993). https://doi.org/10.1016/0022-3115(93)90270-9
9. I.M. Neklyudov, L.S. Ozhigov, A.A. Parkhomenko, and V.F. Stefanov, *Preprint 'Kharkov Institute of Physics and Technology' of the AS of Ukr.SSR*, (Kharkov: 1988), p. 38–53 (in Russian).
10. E. Lopez Sola, M. Calviani , P. Avigni, M. Battistin, J. Busom Descarrega, J. Canhoto Espadanal, M.A. Fraser, S. Gilardoni, B. Goddard, D. Grenier, R. Jacobsson, K. Kershaw, M. Lamont, A. Perillo-Marcone, M. Pandey, B. Riffaud, S. Sgobba,

V. Vlachoudis, and L. Zuccalli, *Phys. Rev. Accel. Beams*, **22**: 113001 (2019). https://doi.org/10.1103/PhysRevAccelBeams.22.113001
11. V. Barabash, G. Federici, M. Rödig, L.L Snead, and C.H. Wu, *J. Nuclear Mater.*, **283–287**, Pt. 1: 138 (2000). https://doi.org/10.1016/S0022-3115(00)00203-8
12. I.M. Neklyudov, L.S. Ozhigov, A.A. Parkhomenko, and M.P. Zeydlits, *Materials of the 2nd Int. Conf. 'High Purity Materials'* (Kharkiv: NSC 'KIPT': 2013), p. 27 (in Russian).
13. A. Hasegawa, M. Fukuda, K. Yabuuchi, and S. Nogami, *J. Nuclear Mater.*, **471**: 175 (2016). https://doi.org/10.1016/j.jnucmat.2015.10.047
14. X. Hu, *J. Nuclear Mater.*, **568**: 153856 (2022). https://doi.org/10.1016/j.jnucmat.2022.153856
15. R.G. Abernethy, J.S.K.-L. Gibson, A. Giannattasio, J.D. Murphy, O. Wouters, R. Bradnam, L.W. Packer, M.R. Gilbert, M. Klimenkov, M. Rieth, H.C. Schneider, C.D. Hardie, S.G. Roberts, and D.E.J. Armstrong, *J. Nuclear Mater.*, **527**: (2019). https://doi.org/10.1016/j.jnucmat.2019.151799
16. A. Mc Clintock, B.J. Vevera, B.W. Riemer, F.X. Gallmeier, J.W. Hyres, and P.D. Ferguson, *J. Nuclear Mater.*, **450**, Nos. 1–3: 130 (2014). https://doi.org./10.1016/j.jnucmat.2014.02.037
17. V.V. Gann, A.V. Gann, B.V. Borts, I.M. Karnaukhov, P.I. Gladkikh, and A.A. Parkhomenko, *Problems of Atomic Science and Technology*, No. 6 (136): 17 (2021). https://doi.org./10.46813/2021-136-017
18. V.V. Gann, A.V. Gann, B.V. Borts, I.M. Karnaukhov, and A.A. Parkhomenko, *Problems of Atomic Science and Technology*, No. 2 (132): 24 (2021). https://doi.org/10.46813/2021-132-024
19. F. Sordo, Radiation Damage Analysis for the ESS Target, *Technical Report ESS-0037287*, European Spallation Source ERIC, 2016.
20. J. Habainy, Y. Lee, K.B. Surdelli, A. Prosvetov, P. Simon, S. Iyengar, Y. Dai, and M. Tomut, *Nuclear Instr. Methods Phys. Res. B*, **439**: 7 (2019). https://doi.org/10.1016/j.nimb.2018.11.017
21. V.V. Gann, I.S. Guk, A.N. Dovbnya, A.I. Kalinichenko, S.G. Kononenko, and A.S. Tarasenko, *Visnyk KhNU, Ser. Fiz. 'Yadra, Chastynky, Polya'*, **868**: 40 (2009) (in Russian).
22. B.V. Borts, A.A. Parkhomenko, I.A. Vorobiev, A.A. Lopata, V.A. Aleksandrov, and M.P. Domnich, *Open J. Metals*, **8**, No. 3: 55 (2018). https://doi.org/10.4236/ojmetal.2018.83004
23. A.S. Drachinskiy, A.V. Krainukov, and V.I. Trefilov, *Fiz. Met. Metalloved.*, **54**: 1133 (1982) (in Russian).
24. D.A. Robins, *J. Less-Common Metals*, **1**, No. 5: 396 (1959). https://doi.org/10.1016/0022-5088(59)90043-8
25. G.V. Samsonov, I.F. Pryadko, and L.F. Pryadko, *Ehlektronnaya Lokalizatsiya v Tverdom Tele* [Electron Localization in Solid] (Moskva: Nauka: 1976 (in Russian).
26. V.G. Glushchenko, *Metallovedenie i Termoobrabotka Metallov*, **4**: 2 (1982). (in Russian).
27. V.I. Trefilov, Yu.V. Milman, and S.A. Firstov, *Fizicheskie Osnovy Prochnosti Tugoplavkikh Metallov* [Physical Principles of Strength of Refractory Metals] (Kiev: Naukova Dumka: 1975) (in Russian).
28. N.A. Azarenkov, A.A. Parkhomenko, L.S. Ozhigov, V.G. Kirichenko, and S.V. Litovchenko, *Materials of the 17th Int. Conf. 'Reactor Materials Science'* (Kharkov: NSC 'KIPT': 2006), p. 39 (in Russian).
29. Y. Kitsunai, H. Kurishita, H. Kayano, Y. Hiraoka, T. Igarashi, and T. Takida, *J.*

Nuclear Mater., **271–272**: 423 (1999).
https://doi.org/10.1016/S0022-3115(98)00753-3
30. B.V. Borts, A.Yu. Zelinsky, A.A. Parkhomenko, V.I. Sytin, L.I. Gluschenko, V.I. Tkachenko, I.A. Vorobyov, A.D. Pidlisnyi, A.A. Lopata, M.P. Domnich, and I.V. Patochkin, *Problems of Atomic Science and Technology*, No. 2 (138): 92 (2022). https://doi.org/10.46813/2022-138-092
31. B.V. Borts, I.A. Vorobyov, A.Yu. Zelinsky, I.M. Karnaukhov, A.A. Lopata, A.A. Parkhomenko, I.V. Patochkin, and V.I. Tkachenko, *Problems of Atomic Science and Technology*, No. 2 (144): 58 (2023).
https://doi.org/10.46813/2023-144-058

Received 28.06.2024
Final version 09.08.2024

Б.В. Борц, О.О. Пархоменко, В.В. Ганн, А.Ю. Зелінський, В.І. Ситін, І.О. Воробйов, Л.І. Глущенко, І.І. Карнаухов, Ю.О. Марченко, М.П. Домніч
Національний науковий центр «Харківський фізико-технічний інститут» НАН України,
вул. Академічна, 1, 61108 Харків, Україна

ВЛАСТИВОСТІ МАТЕРІАЛІВ W–Ta НЕЙТРОНОУТВОРЮВАЛЬНОЇ МІШЕНІ ПІДКРИТИЧНОГО СКЛАДЕННЯ ННЦ «ХФТІ» НАН УКРАЇНИ

Наведено огляд праць у галузі радіаційного матеріалознавства матеріалів мішеней джерел нейтронів на основі докритичних складень, керованих лінійними пришвидшувачами електронів або протонів, — так званих систем ADS (accelerator driven systems — керовані пришвидшувачем системи). На сьогодні електроядерні системи ADS є прототипом безпечних ядерних реакторів 5-го покоління. У зв'язку з фізичним пуском установки джерела нейтронів ННЦ «ХФТІ» НАН України, мішень якої виготовляється з порошкоподібного вольфраму, покритого танталом, розглянуто питання технології виготовлення, конструкції та фізико-механічних властивостей W–Ta-матеріалів мішеней в неопроміненому й опроміненому станах. Проаналізовано ядерно-фізичні процеси радіаційного ураження мішені під час її спільного опромінювання нейтронами субкритичного складення і високоенергетичними *e*- та γ-пучками. Оцінено цільові ресурси систем ADS. Відзначено, що складність прогнозування «живучості» W–Ta-мішені, оскільки, що, за винятком досліджень, проведених у ННЦ «ХФТІ» НАН України в 70–90-х роках минулого сторіччя, у світі немає експериментальних робіт з радіаційного ураження матеріалів реакторів високоенергетичними електронами з енергією у 100 МеВ і вище.

Ключові слова: субкритичні ядерні системи, вольфрам-танталові мішені, високотемпературне вакуумне прокатування, механічні властивості, металографія, нано та мікротвердість, ступінь пошкодження, радіаційна крихкість, ресурс.